ACS Sustainable Chemistry & Engineering

Research Article

Cite This: ACS Sustainable Chem. Eng. 2019, 7, 19050−19061

pubs.acs.org/journal/ascecg

Self-Catalyzed Coupling between Brønsted-Acidic Imidazolium Salts and Epoxy-Based Materials: A Theoretical/Experimental Study

Magdalena Perchacz,[†,‡] Libor Matějka,[†] Rafał Konefał,[†] Leandro Seixas,[§] Sebastien Livi,[∥] Jérôme Baudoux,[⊥] Hynek Beneš,*[,†] and Ricardo K. Donato*[,†]

[†]Institute of Macromolecular Chemistry, Czech Academy of Sciences, Heyrovského nám. 2, 162 06 Prague 6, Czech Republic

[‡]Centre of Molecular and Macromolecular Studies, Polish Academy of Sciences, Sienkiewicza 112, 90-363 Łódź, Poland

[§]MackGraphe—Graphene and Nanomaterials Research Centre, Mackenzie Presbyterian University, Rua da Consolação 896, São Paulo, São Paulo 01302-907, Brasil

[∥]Université de Lyon, INSA Lyon CNRS, UMR 5223, Ingénierie des Matériaux Polymères, F-69003 Lyon, France

[⊥]Laboratoire de Chimie Moléculaire et Thio-organique, ENSICAEN, Université de Normandie, CNRS, 6 boulevard du Maréchal Juin, 14050 Caen, France

Supporting Information

ABSTRACT: Herein we present a comprehensive study on the role of Brønsted-acidic imidazolium ionic liquids (ILs) and imidazolium salts promoting the reaction between carboxyl and epoxide groups in a controlled manner at solvent-free and mild conditions. ILs were evaluated toward their ability to self-catalyze reactions between carboxyl groups and epoxy rings. Thus, an epoxy model reactant denoted phenyl glycidyl ether (PGE) was reacted with different ILs, and the reaction kinetics was followed by time-dependent FTIR spectroscopy. The resulting products were characterized by ^{1}H NMR and MALDI-TOF, which also allowed a comprehensive investigation of the reaction mechanism by following the reaction intermediates formation. The detected intermediates were then evaluated by density functional theory (DFT) simulations to calculate their energy profiles, revealing the preferred mechanism pathways. These mono-, bi-, and tetra-functionalized ILs (with carboxyl groups) acted as all-in-one reaction systems for materials synthesis or modification, with the potential of producing a broad range of epoxy based materials via metal catalyst-free coupling reactions.

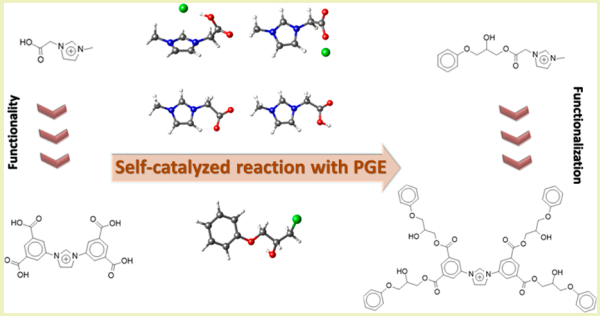

KEYWORDS: *Ionic liquid, Catalysis, One-pot reaction, Ring-opening, Mechanism, Solvent-free*

INTRODUCTION

The reactions between epoxy and carboxyl moieties are extremely interesting, especially due to the abundance of these functional groups in nature and consequent potential for obtaining/modifying diverse products based on natural monomers/polymers. However, their chemistry is generally complicated to achieve under strict control and is governed by four main reactions: (1) addition esterification of carboxylic acids (C) and epoxy rings (E), forming a hydroxymonoester (M); (2) etherification (E + M, homopolymerization); (3) esterification between carboxylic acid and hydroxymonoester (C + M) forming a diester (D); and (4) a reversible transesterification (M + M) forming D and glycol. Under stoichiometric conditions, the monoester formation is favored (1), since the etherification (2) and condensation esterification (3) are much slower and appear only at the nonstoichiometric compositions. However, once the formation of monoester is promoted the reversible transesterification (4) occurs to form diester and glycol even under stoichiometric conditions.[1] Recently, the control of these reactions has been receiving especial attention for preparing polymer networks with thermoplastic/thermoset behavior due to the labile and thermosensitive nature of these bonds, which allow the formation of vitrimers.[2]

Similarly complex are the reaction mechanisms between epoxide groups and the imidazolium cation of salts and ionic liquids (ILs). ILs are organic salts with ionocovalent structures, remaining as liquids in a broad temperature range below 100 °C. They present a quite impressive set of properties, including; extremely low vapor pressure and insignificant flammability, high thermal and chemical stability, wide electrochemical windows, good thermal conductivity, high ionic mobility and stability in the presence of air and moisture, etc.[3,4] As proposed by Maka et al., the ILs' deprotonation, dealkylation, decomposition, and/or fragmentation form nucleophilic imidazole species, which promote the epoxide

Received: August 19, 2019
Revised: October 17, 2019
Published: October 31, 2019

DOI: 10.1021/acssuschemeng.9b04810
ACS Sustainable Chem. Eng. 2019, 7, 19050−19061

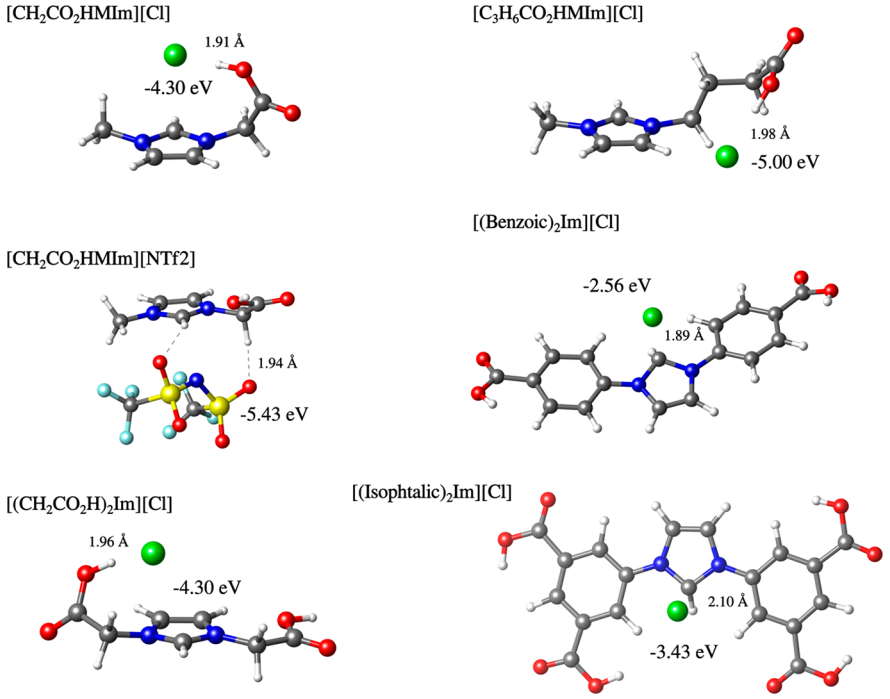

Figure 1. Ball-and-stick representation of the ILs studied, showing their structure, length of the shortest bond, and binding energy (between the cation/anion pair) at the relaxed state, as obtained by DFT simulations. Carbon atoms are represented in gray, oxygen in red, nitrogen in blue, hydrogen in white, sulfur in yellow, fluorine in cyan, and chlorine in green.

ring-opening.[5,6] However, this approach is mostly justified by the high temperatures or basic conditions, required for processing of the resulting networks, while their mechanism at lower temperatures are not clearly understood. Accordingly, recently we have reported that some imidazolium ILs do not cause epoxide ring-opening when used at relatively low temperatures (80 °C) in the alkoxysilane-based sol−gel process.[7] Moreover, they led to the formation of well-structured silica xerogels, based on 3D cages, containing fully reactive oxirane rings easily miscible with the epoxy-amine network.

Taking that into account, once the previously discussed hurdles are overcome, the introduction of these ionic structures into polymer systems could be an interesting alternative to produce reinforced but labile interphases. The introduction of ionicity into polymer nanocomposites and blends interphases, especially in the presence of other physical interactions, has been recently demonstrated as a practical option for obtaining high performance smart materials.[8,9] Partially ionic materials produce complex ionic and multiple hydrogen-bonding (H-bond) nanocomposite interphases that allow controlling the nanocomposite structure, morphology, and properties in different matrices and processes.[10,12−17] Also due to the bond lability produced, they avoid the usual brittleness at lower temperatures,[8] additionally exhibiting properties such as shape-memory and self-healing.[8,10,11,18,19]

Using a similar approach, previously we observed that carboxy-functionalized ILs (carboxylic-IL) presented selective high reactivity with epoxy-based compounds, even in viscous and complex epoxy−silica nanocomposite systems, forming nanocomposites with dramatically improved mechanical properties with the addition of very small amounts of IL (~0.2 wt %).[20] However, previously we could not fully explain the organic/inorganic interface modification process induced by the carboxylic-ILs. Thus, herein, the reactivity of different carboxylic-ILs toward an epoxy species was studied, aiming for better understanding the reaction mechanism and structural dependency of carboxylic-ILs to be self-catalyzed (Figure 1). In order to simplify the characterization and give a better idea of the polymerization/reticulation steps, the monofunctional epoxy molecule Phenyl glicydyl ether (PGE) was used, as it presents a very similar reactivity to standard epoxy precursors (e.g., diglicydyl ether of bisphenol A).[21] The reaction between PGE and the different carboxylic-ILs was investigated using FTIR, enabling us to follow the epoxide group consumption as a function of time. The obtained experimental data were further compared with the final relaxed structures and their energy profiles, as calculated by density functional theory (DFT) simulations. The final products, after epoxide group consumption, were characterized by ^{1}H NMR and MALDI-TOF, and the results were used to perform a comprehensive (IL) structure−mechanism correlation study.

EXPERIMENTAL SECTION

Materials. All reagents were purchased from Sigma-Aldrich, Alfa Aesar, or TCI and were used as-received, without further purification. Anhydrous solvents were obtained from a PURESOLV SPS400 apparatus developed by Innovative Technology Inc.

Imidazolium Salts and Ionic Liquids. The 1-butyl-3-methyl imidazolium chloride (C_4MImCl, ≥99% Sigma-Aldrich) IL was purchased from Sigma-Aldrich and used without any previous treatment. The 1-carboxymethyl-3-methylimidazolium chloride (CH_2CO_2HMImCl), 1-carboxypropyl-3-methylimidazolium chloride ($C_3H_6CO_2$HMImCl), and 1,3-dicarboxymethylimidazolium chloride $(CH_2CO_2H)_2$MImCl ILs, were synthesized as described in the literature.[22] The 1-carboxymethyl-3-methylimidazolium bis (trifluoromethyl-sulfonyl) imide (CH_2CO_2HMImNTf$_2$) IL was prepared by anion exchange from its Cl^- correlate (CH_2CO_2HMImCl). The latter was performed by mixing CH_2CO_2HMImCl together with lithium bis(trifluoromethylsulfonyl)amide (LiNTf$_2$, 99% Sigma-Aldrich) (1/1.05 molar ratio) in dichloromethane, and stirring for 48 h. The

DOI: 10.1021/acssuschemeng.9b04810
ACS Sustainable Chem. Eng. 2019, 7, 19050−19061

Table 1. Summary of Coupling Reaction Yields Based on MALDI-TOF

	unreacted IL species	reaction products			
	yield [ref peak (m/z)][a]	yield [ref peak (m/z)][a]			
PGE+IL		mono	di	tri	tetra
$CH_2CO_2HMImCl$ (25 °C)	**54%** [16% (141)]; [35% (281)]; [4% (421)]	[22% (291)]; [24% (431)]	**46%**		
$CH_2CO_2HMImCl$ (100 °C)	**8%** [4% (141)]; [4% (281)]	[60% (291)]; [29% (431)]	**92%** [4% (413)]		
$CH_2CO_2HMImNTf_2$ (25 °C)	**13%** [13% (141)]	[73% (291)]; [6% (431)]	**87%** [6% (441)]	[2% (591)]	
$C_3H_6CO_2HMImCl$ (25 °C)	**78%** [58% (169)]; [20% (337)]	[9% (233)]; [10% (319)]; [3% (487)]	**22%**		
$C_3H_6CO_2HMImCl$ (100 °C)	**8%** [4% (169)]; [4% (337)]	[8% (233)]; [79% (319)]; [5% (487)]	**92%**		
$(CH_2CO_2H)_2ImCl$ (25 °C)	**95%** [50% (185)]; [31% (369)]; [10% (553)]; [4% (737)]	[5% (335)]	**5%**		
$(CH_2CO_2H)_2ImCl$ (100 °C)	**55%** [11% (185)]; [44% (369)]	[18% (335)]	**45%** [27% (485)]		
$(Benzoic)_2ImCl$ (100 °C)	**29%** [29% (309)]	[38% (459)]	**71%** [33% (609)]		
$(Isophtalic)_2ImCl$ (100 °C)	**16%** [16% (397)]	[8% (547)]	**84%** [11% (697)]	[25% (847)]	[40% (997)]

[a]Determined by the total absorbance correlation between the MALDI-TOF peaks assigned, excluding matrix interferences and artifacts.

DOI: 10.1021/acssuschemeng.9b04810
ACS Sustainable Chem. Eng. 2019, 7, 19050−19061

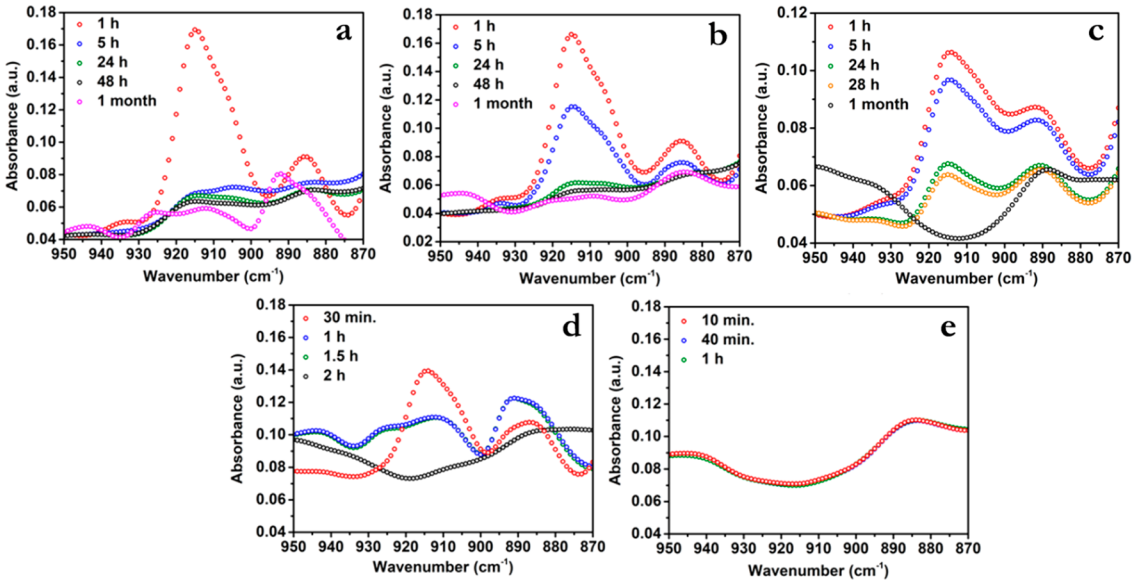

Figure 2. FTIR spectra presenting kinetics of PGE's epoxide ring-opening with $CH_2CO_2HMImCl$ (a), $C_3H_6CO_2HMImCl$ (b), and $CH_2CO_2HMImNTf_2$ (c) at 25 °C; and with $CH_2CO_2HMImCl$ (d) and $C_3H_6CO_2HMImCl$ (e) at 100 °C.

precipitated LiCl salt was removed by filtration and $CH_2CO_2HMImNTf_2$ was obtained after solvent removal under vacuum. Their purities were checked by ^{1}H NMR and ^{13}C NMR, and were in accordance with published data. The 1,3-bis(4-carboxyphenyl)imidazolium chloride ($(Benzoic)_2ImCl$) and 1,3-bis(3,5-dicarboxyphenyl)imidazolium chloride ($(Isophtalic)_2ImCl$) were also synthesized as described in the literature[23,24] with a few adaptations (details in the Supporting Information, SI), their purities were checked by ^{1}H NMR, ^{13}C NMR, and MALDI-TOF, and were in accordance with published data (SI Figures S1–S6).

Epoxy-Carboxylic Acid Model Reaction. In order to evaluate the epoxide ring-opening mechanism of phenyl glycidyl ether (PGE), initiated by the carboxy-functionalized ILs, model reactions between both components, used in stoichiometric ratio of functional groups (1.0 mmol), were performed at 25 °C as well as at 100 °C. For better dispersion of ILs and PGE at 25 °C, the mixtures were initially treated in an ultrasound bath (320 W) for 3 min. The process of PGE's epoxide ring-opening was followed using FTIR measurements of aliquots collected during the reaction, while the final products were characterized by ^{1}H NMR and MALDI-TOF.

Additionally, we performed reactions, at 25 °C, between PGE and acetic acid with/without addition of C_4MImCl (as a nonfunctionalized IL), in the following molar ratios; acetic acid/PGE (1/1) and acetic acid/C_4MImCl (1/0.3 and 1/1).

Methods. *Density Functional Theory.* The computational approach was based on density functional theory (DFT) as implemented in SIESTA code.[25] We used triple-ζ basis set with polarization orbitals (TZP), norm-conserved Troullier-Martins pseudopotentials,[26] and mesh cutoff of 400 Ry. The exchange-correlation functional is in Vydrov-van Voorhis (VV10) approximation.[27] All the structures were optimized until the forces were smaller than 0.040 eV/Å. Binding energies were calculated with Boys–Bernardi counterpoise method for basis set superposition error correction.[28]

Infrared Spectroscopy. The infrared (FTIR) spectra of the products were measured using a Spectrum 100 spectrometer (PerkinElmer) equipped with a mercury–cadmium–telluride (MCT) detector and universal ATR (attenuated total reflectance) accessory with a diamond prism. The spectra were averaged over 32 scans with selected resolution of 4 cm^{-1}. The progress of the epoxide-IL reaction was monitored as for the disappearance of the peak at ~915 cm^{-1} corresponding to the C–O stretching of epoxide group.[29]

Nuclear Magnetic Resonance. ^{1}H NMR spectra were acquired with Bruker Avance III 600 spectrometer operating at 600.2 MHz with C_2D_5OD as the solvent at 295 K. The width of 90° pulse was 10 μs with relaxation delay 10 s. The acquisition time was 2.18 s with 16–32 scans. The chemical shifts are relative to TMS using hexamethyldisiloxane (HMDSO, 0.05 ppm from TMS in ^{1}H NMR spectra) as internal standard.

Matrix-Assisted Laser Desorption/Ionization-Time-of-Flight Mass Spectrometry (MALDI-TOF). MALDI-TOF mass spectra were acquired with an Ultraflex (Bruker Daltonics, Bremen, Germany) in the positive ion reflection mode, using delayed extraction. The spectra were the result of averaged values of 3 measurements, each from the sum of 30 000 shots with a DPSS, Nd: YAG laser (355 nm, 1000 Hz). External calibration was used.

The samples were prepared by the dried droplet method. Dimethylformamide (DMF) solutions of the sample (10 mg/mL), the matrix: DHB (2,5-dihydroxybenzoic acid; 20 mg/mL), and the cationization agent: sodium trifluoroacetate ($NaCF_3COO$; 10 mg/mL) were mixed in the respective volume ratio 4:20:1.1 μL. The mixture was deposited on a ground-steel target plate, and the analyte drop was dried at ambient atmosphere.

RESULTS AND DISCUSSION

As previously described by Binks et al.,[30] ILs with halide anions can induce a complex anionic initiation mechanism, where one of the possible rotes is, as they refer to, a "counter ion route". More specifically for Brønsted-acidic ILs, Ranu et al. also described a mechanism for the cleavage of epoxides to halohydrins without requirement of any other catalyst or solvent.[28] In their proposed mechanism, besides the halohydrins, also a zwitterionic species derived from the original IL should be formed (vide infra). However, the referred work did not present any correlated discussion.

Since we have been investigating the chemical insertion of the imidazolium cation into the epoxy network, this work comprises a detailed study on the IL's reactivity in relation to their chemical structure. Different Brønsted-acidic ILs varying the number of functional carboxyl groups per imidazolium unit (from mono- to tetra-functionalized) and the steric nature of both cation and anion were selected (Figure 1).

Reactivity of ILs in Relation to Their Functionality. For a better understanding the extent of self-catalyzing capacity of the ILs, the characterizations and discussions of the PGE-IL

DOI: 10.1021/acssuschemeng.9b04810
ACS Sustainable Chem. Eng. 2019, 7, 19050–19061

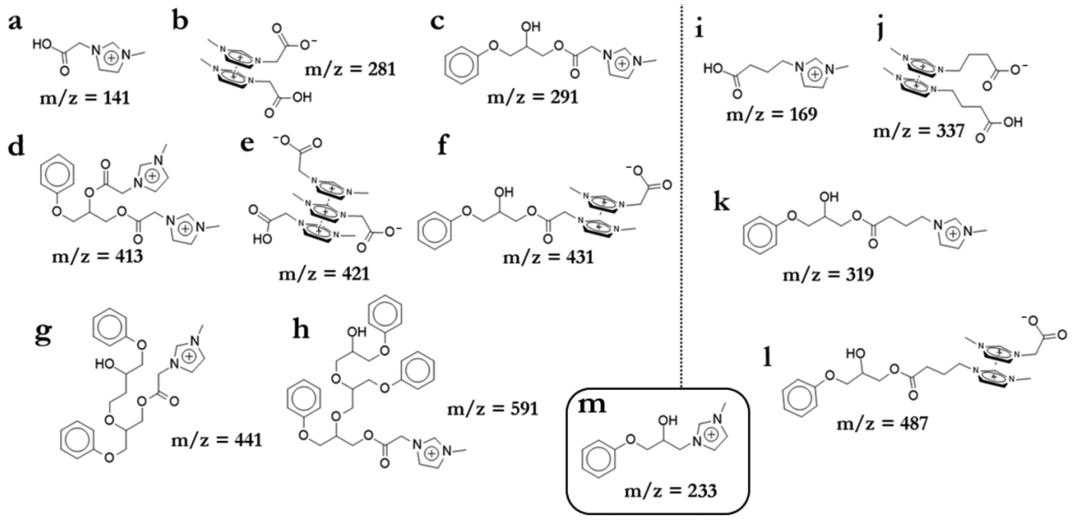

Figure 3. Structures detected by MALDI-TOF in the systems derived from the reaction between PGE and $CH_2CO_2HMImCl$ at 25 °C (a–c, e–g), $CH_2CO_2HMImCl$ at 100 °C (a–d, f), $CH_2CO_2HMImNTf_2$ at 25 °C (a, c, f–h), $C_3H_6CO_2HMImCl$ at 25 °C (i–m), and $C_3H_6CO_2HMImCl$ at 100 °C (i–m).

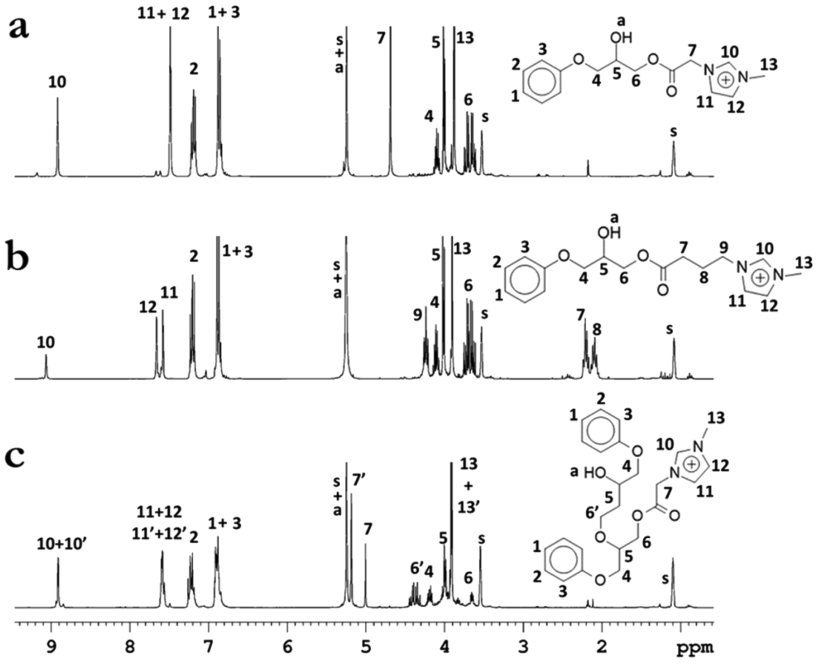

Figure 4. ^1H NMR spectra of reactions (at 25 °C) between PGE and $CH_2CO_2HMImCl$ (a), $C_3H_6CO_2HMImCl$ (b), and $CH_2CO_2HMImNTf_2$ (c). Signals were assigned as *n′* when the same proton presented different field shifted signals between reactant and product or between different adducts.

systems were segregated based on the number of functional groups per imidazolium unit. Moreover, due to the large number of overlapped bands among the system components, time-dependent FTIR was used mainly to evaluate (semi-quantitatively) the oxirane ring band consumption, and the formation of ether/ester bonds (C–O bands) and stable carboxylate anions (O–C–O$^-$ band).[32] The final product conversions were calculated using NMR and MALDI-TOF. NMR was also used to evaluate the PGE oxirane ring consumption, to match FTIR results, and detect the PGE-IL coupling reaction products, while MALDI-TOF was used to evaluate the ratio between unreacted and reacted IL-cations (since it was measured in positive-ion mode) by perfectly matching their masses (all results are summarized in Table 1, considering the peaks' intensity contributions). All the FTIR, NMR, and MALDI-TOF supporting data are presented in the SI and are systematically referred throughout the text.

Monofunctional ILs. When considering the reactions at 25 °C, the fastest epoxide ring opening processes were observed for the systems with both monofunctional ILs containing the chloride anion (Cl^-) ($CH_2CO_2HMImCl$ and $C_3H_6CO_2HMImCl$). $CH_2CO_2HMImCl$ caused higher epoxy consumption than $C_3H_6CO_2HMImCl$ only at the beginning of the reaction, which could be due to its better solubility/dispersion in the reaction system (as observed during the reaction). Despite the quite different oxirane ring consumption after 5 h, $CH_2CO_2HMImCl$ and $C_3H_6CO_2HMImCl$ revealed a very similar efficiency after 48 h of reaction (Figures 2a and b

DOI: 10.1021/acssuschemeng.9b04810
ACS Sustainable Chem. Eng. 2019, 7, 19050–19061

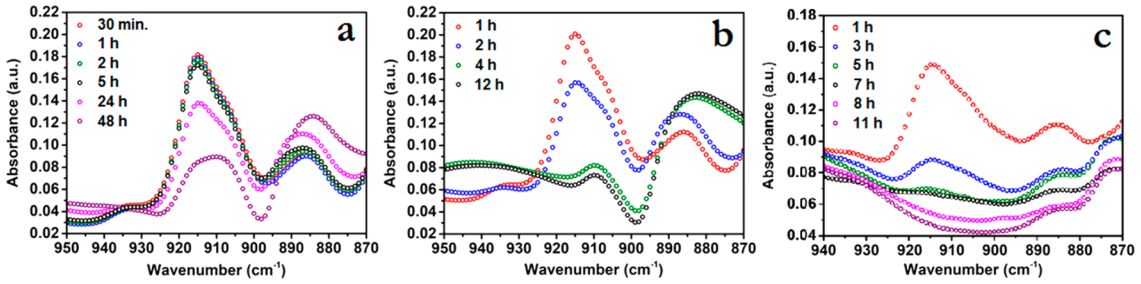

Figure 5. FTIR spectra presenting the kinetics of the reaction between; PGE and $(CH_2CO_2H)_2$ImCl at 25 °C (a) and 100 °C (b); and PGE and $(Benzoic)_2$ImCl at 100 °C (c).

and 3). Accordingly, the ^{1}H NMR and MALDI-TOF measurements (after 48 h reaction) showed epoxy consumption of ∼98% and 100% (absence of ^{1}H NMR peaks related to the residual oxirane rings at $\delta \approx 2.8$ ppm, Figure 4a and b), while only about 46% and 22% (Figures S14 and S15) converted into the PGE-IL coupling products (Figure 3c, f, k, and l), for the systems containing CH_2CO_2HMImCl and $C_3H_6CO_2$HMImCl, respectively. Despite the good reactivity of the ILs, the majority of these ILs' cations remained in their monomeric form (Figure 3a and (i), stacked clusters partially stabilizing their zwitterionic species formed by the loss of the carboxyl proton (Figure 3b, e, and j) or zwitterionic species stabilized by the coupling product (Figure 3f and l).

The IL stacking via hydrogen bonding, C−H−π interactions and $\pi-\pi$ stacking could be clearly evidenced by the higher field shifted "satellite" signals of the imidazolium ring (Figures 4 and S7; signals 8′, 9′, 10′, 11′) and decreased signal 8 (related to the C2 hydrogen).[33−35]

Moreover, the size of stacked clusters could be determined by MALDI-TOF, since their exact mass matches perfectly with the structure of clusters composed of IL cation (e.g., m/z = 141 for CH_2CO_2HMImCl) and multiple deprotonated IL cations forming zwitterions (e.g., structures at Figure 3b, e, and j). Interestingly, the sizes of these clusters vary with the IL structure, but with a common feature of always presenting a total charge +1 due to the presence of one unaltered cationic species. Finally, the presence of the carboxylate anion (as evidence for the zwitterion formation) could also be observed by FTIR, as the suppression in the C═O vibrational mode (∼1710 cm^{-1}) and appearance of a new band at lower wavenumber (∼1615 cm^{-1}, Figure S12),[32] which is often observed in amino acids in the zwitterion form.[36] It is worth noting that these stacked structures are also present in the neat IL structures (Figures S5 and S6), showing that it is a natural self-stabilizing tendency of this type of IL.

However, the reaction at 25 °C between PGE and CH_2CO_2HMImNTf$_2$, containing the bulkier anion bis-(trifluoromethylsulfonyl)amide (NTf$_2^-$), presented a different behavior compared to its Cl$^-$ anion correlate. Besides the apparently slower oxirane ring band disappearance (Figure 2c), and no O−C−O$^-$ band formation (Figure S12), a ^{1}H NMR signal (7′) related to the neat CH_2CO_2HMImNTf$_2$ was observed (Figure 4c), indicating a small amount of unreacted IL in the final product. Moreover, the reaction between PGE and CH_2CO_2HMImNTf$_2$ also led to the formation of small amounts (about 9% of the total reacted IL) of dimers and trimers of PGE via etherification reaction (Figure 3g and h), which could be detected by both ^{1}H-NMR (Figure 4c) and MALDI-TOF (Figure S14). These results suggest the presence of more than one reaction mechanism between PGE and the ILs, and a major influence of the IL's anion on the reaction mechanisms, most probably presenting a role as a nucleophile that initiates the ring-opening reaction.

As expected, when the reactions were performed at 100 °C, they proceeded in a much faster rate for both carboxylic-ILs with Cl$^-$ anion (compare Figure 2a vs d and Figure 2b vs e). In this case, the fastest reaction was for the system containing $C_3H_6CO_2$HMImCl, which could be a consequence of its improved solubility/diffusion with increasing the temperature, leading to a higher reactivity with the epoxide groups. At this temperature, after only 10 min of the reaction, all the epoxide groups of PGE were consumed, as evidenced by FTIR (Figure 2e) and ^{1}H NMR (Figure S8), and about 92% (MALDI-TOF) of the IL reacted with PGE (Figures 3k and S15). Such behavior corroborate with our previous results,[20] concerning the formation of the most reinforced organic/inorganic interphase in epoxy-silica nanocomposites modified by $C_3H_6CO_2$HMImCl. It is worth noting that specifically for the reactions between the PGE and $C_3H_6CO_2$HMImCl, in both temperatures, also a coupling product between an imidazolium ring and PGE was detected in small amounts (Figure 3m). This could indicate that, despite the mild temperatures, some IL decomposition via C−N bond cleavage is produced during the reaction process, allowing then the imidazole N atom nucleophilic attack to PGE.[37]

CH_2CO_2HMImCl also led to a considerable increase in reaction rate at 100 °C, with total oxirane ring consumption after 2h (Figures 2d and S7), and about 92% of PGE-IL coupling reaction (Figure S14). Interestingly, exclusively the reaction between PGE and CH_2CO_2HMImCl at 100 °C, presented a small amount of structures formed after a second cation insertion, probably via transesterification or condensation esterification reaction (Figure 3d). However, transesterification could not be proved since the formation of glycol was not detectable by MALDI-TOF in positive ionization mode.

Difunctional ILs. In order to unveil the influence of the number of IL's carboxyl groups on both epoxide ring-opening and coupling processes, the reactions between PGE and two difunctional ILs ($(CH_2CO_2H)_2$ImCl and $(Benzoic)_2$ImCl) were also performed. The structural differences between $(CH_2CO_2H)_2$ImCl and $(Benzoic)_2$ImCl also allowed evaluating the influence of the ILs' cation side-chain mobility (aliphatic vs aromatic) on the reaction.

Although the $(CH_2CO_2H)_2$MImCl reacted with PGE at 25 °C, at this temperature the reaction medium presented some turbidity, suggesting lack of solubility, what reflected on the reaction yield. The FTIR spectra showed a large fraction of unreacted epoxy species and zwitterionic IL formation (Figures 5a and S13), which was confirmed by MALDI-TOF showing

DOI: 10.1021/acssuschemeng.9b04810
ACS Sustainable Chem. Eng. 2019, 7, 19050−19061

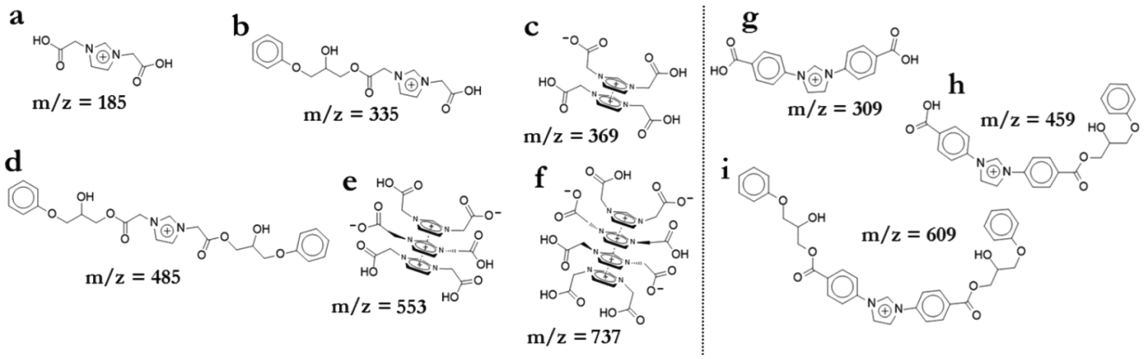

Figure 6. Structures detected by MALDI-TOF in the system derived from the reaction between PGE and $(CH_2CO_2H)_2$ImCl at 25 °C (a–c, e, f) and 100 °C (a–d) and $(Benzoic)_2$ImCl at 100 °C (g–i).

only about 5% of PGE-IL coupling reaction product (limited to the reaction with only one of the carboxyl groups, Figure 6b) and a large amount of unreacted IL and its stacked structures (Figures 6a, c, e, and f and S16). The lack of solubility (and consequent turbidity) did not allow for a reliable NMR characterization of this system.

Only at 100 °C the PGE-$(CH_2CO_2H)_2$ImCl reaction presented a much faster rate and the consumption of the majority of PGE's oxirane rings in about 12 h (Figure 5b). Moreover, ^{1}H NMR analysis confirmed ∼98% epoxide ring consumption, and the two main products (mono- and disubstituted, Figure 6b and d) of the reaction were detected. Their structures and signal assignments were presented in the SI (Figure S9), where the ratio between the mono- (signals 6, 7, 8, 9, 10) and the disubstituted (signals 6′, 7′, 8′, 9′, 10′) products was calculated from the ratios of the integrals of peaks 8:8′ and 6:6′, and amounted to a 30:70 ratio, respectively. These results were also confirmed by MALDI-TOF, since about 45% of the IL produced coupling reaction products, from which 60% had both carboxylic groups reacted with two PGE molecules (Figures 6d and S16).

The reaction between PGE and $(Benzoic)_2$ImCl was only characterized and discussed when performed at 100 °C, since at 25 °C the miscibility with PGE was so low that promoted the IL's precipitation. However, at 100 °C, $(Benzoic)_2$ImCl caused an efficient PGE's epoxy groups consumption (Figure 5c), with about 98% epoxide ring-opening (Figure S10) and about 71% of those converted to the coupling products (Figures 6h and i, and S17). The IL $(Benzoic)_2$ImCl also produced the mono- and disubstituted IL (Figure 6h and i), and the ratio between mono- (7′, 8′, 9′, 10′) and disubstituted products (7, 8, 9, 10) was calculated (by NMR) from the ratios between the integrals of the peaks 7′:7, and amounted to 22:78, respectively (Figure S10). Interestingly, although $(Benzoic)_2$ImCl presents many p-orbitals for $\pi-\pi$ stacking, the structural aggregates were neither detected by FTIR (Figure S13) nor by MALDI-TOF (Figure S17). This could be caused by the molecular rigidity of the aromatic six-membered rings, decreasing the aggregation and leading to higher reactivity with the epoxide groups.

Tetrafunctional IL. The introduction of two isophtalic substituents into an imidazolium ring allowed obtaining an IL with four carboxyl groups ($(Isophtalic)_2$ImCl). Similarly to the $(Benzoic)_2$ImCl, the reaction between this IL and PGE was only characterized and discussed at 100 °C due to the lack of solubility in the reaction medium at 25 °C.

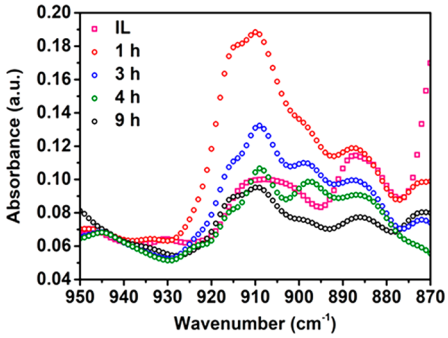

Figure 7. FTIR spectra presenting kinetics of PGE's epoxide ring-opening reaction at 100 °C, induced by $(Isophtalic)_2$ImCl. The curve labeled as "IL" represents the neat $(Isophtalic)_2$ImCl) overlapping band.

This IL promoted a considerably fast epoxide ring opening, as the majority of oxirane rings were consumed after 9 h of reaction (Figure 7). However, it is worth noting that the $(Isophtalic)_2$ImCl presents a vibrational band at 910 cm^{-1}, which overlaps the C–O stretching band of the oxirane ring and, thus, not allowing observing the total epoxy consumption (Figure 7). Nevertheless, ^{1}H NMR showed that after 12 h the PGE-$(Isophtalic)_2$ImCl system reached ∼70% of the epoxide groups consumption, i.e., about 30% of epoxide groups remained unreacted after the process. Moreover, the large amount of signals at low field region of ^{1}H NMR spectrum ($\delta \approx 7.5-9$ ppm) indicates that a mixture of mono-, di-, tri-, and tetra- substituted products were formed during the reaction (Figure S11). These results were also confirmed by MALDI-TOF (Figure S17), which presented about 16% of unreacted $(Isophtalic)_2$ImCl (Figure 8a), and about 84% coupling reaction products, including the mono- (9.5%, Figure 8b), di- (13%, Figure 8c), tri- (30%, Figure 8d), and tetra-substituted products (48%, Figure 8e). Interestingly the majority of the products were tetra-substituted, representing an interesting system for cross-linked networks.

Also, no etherification or transesterification products were observed for this system, which could be a consequence of the higher steric hindrance of this IL, especially as its tetra-substituted reaction product.

Reaction Mechanism: Understanding the Intramolecular Self-Catalysis. In order to understand the individual roles of functional carboxyl group and IL in the epoxide ring-opening reaction, we also performed experiments with acetic acid, as a carboxylic acid reference, with and without the

DOI: 10.1021/acssuschemeng.9b04810
ACS Sustainable Chem. Eng. 2019, 7, 19050–19061

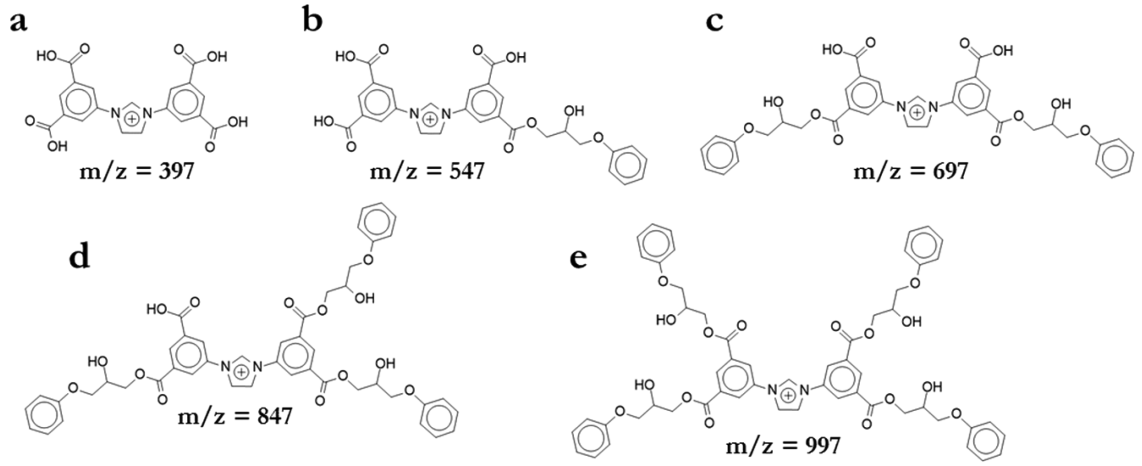

Figure 8. Structures detected by MALDI-TOF in the system derived from the reaction between PGE and (Isophtalic)$_2$ImCl at 100 °C.

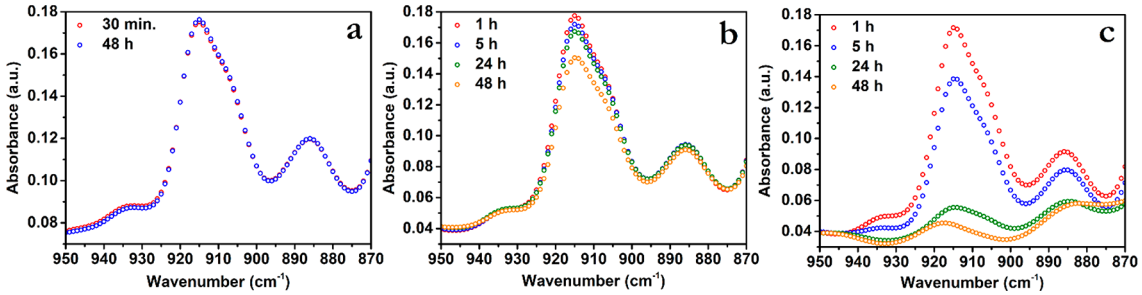

Figure 9. FTIR spectra presenting kinetics of the reactions, at 25 °C, between PGE and acetic acid (a), acetic acid/C_4MImCl (1/0.3 molar ratio) (b), and acetic acid/C_4MImCl (1/1 molar ratio) (c).

Table 2. Chemical Properties of IL's Ion Pairs, Isolated Anion and Cations, and Acetic Acid Molecule As Calculated by DFT[a]

no.	system	d (Å)[b]	E_b (eV)[c]	HOMO (eV)[d]	LUMO (eV)[e]	η (eV)[f]
1	acetic acid			−7.11	−1.87	2.62
2	Cl			−8.31	−7.27	7.79
3	NTf_2			−8.27	−2.95	2.66
4	CH_2CO_2HMIm			−1.91	−1.17	0.37
5	CH_2CO_2MIm			−5.44	−3.76	1.68
6	$CH_2CO_2HMImCl$	1.91	−4.30	−6.41	−3.13	1.64
7	$CH_2CO_2HMImNTf_2$	1.94	−5.43	−7.69	−3.58	2.06
8	$C_3H_6CO_2HMImCl$	1.98	−5.00	−6.24	−4.18	1.03
9	$(CH_2CO_2H)_2ImCl$	1.96	−4.30	−6.44	−3.41	1.52
10	$(Benzoic)_2ImCl$	1.89	−2.56	−5.96	−5.67	0.15
11	CH_2CO_2MImCl	2.58	−1.32	−6.30	−4.14	1.08
12	$(isophtalic)_2ImCl$	2.10	−3.43	−6.54	−4.28	1.13
13	halohydrin intermediate			−5.97	−1.84	2.07

[a]Also, the halohydrin intermediate formed by their reaction, as determined by DFT. [b]Binding distance between anion and cation. [c]Binding energy. [d]Highest occupied molecular orbital energy. [e]Lowest unoccupied molecular orbital energy. [f]Chemical hardness.

addition of a nonfunctionalized IL containing *n*-butyl side-chain (1-butyl-3-methylimidazolium chloride, C_4MImCl). In this manner, the functional group (carboxyl) and the catalyst (IL) were segregated into two different molecules, allowing only the occurrence of intermolecular catalysis.

First, the addition of only acetic acid to PGE did not cause any epoxide ring-opening process, even after long-term exposition (Figure 9a). However, the combination of acetic acid/C_4MImCl (1/0.3 molar ratio) allowed a small oxirane ring consumption (Figure 9b), which was significantly increased when an equimolar acetic acid/C_4MImCl ratio was used (Figure 9c). Such results evidently display the IL's essential role in the epoxide ring-opening reaction, through a mechanism that is dependent on the IL's concentration. As evidence to that assumption, the epoxide ring-opening process at 25 °C was faster in the system containing $CH_2CO_2HMImCl$, compared to the equimolar acetic acid/C_4MImCl system (compare Figures 2a and 9c).

Reaction Mechanism: DFT Investigation of Reaction Intermediates. For better understanding the conditions involved in the ILs' reactivity with PGE, DFT simulations were used for determining the ILs' structural features that increase/decrease their reactivity and compare with the results obtained experimentally. On the basis of total-energy density

DOI: 10.1021/acssuschemeng.9b04810
ACS Sustainable Chem. Eng. 2019, 7, 19050−19061

functional simulations, we have calculated chemical properties such as cation−anion binding energy (E_b),[28] the highest occupied molecular orbital energy (HOMO), the lowest unoccupied molecular orbital energy (LUMO), and chemical hardness (η) of the ILs. These chemical quantities were calculated using eq 1.

$$\eta = (\mathrm{LUMO} - \mathrm{HOMO})/2 \quad (1)$$

The η was evaluated for determining the stability of possible intermediates configurations.

In Table 2, are displayed these quantities for: (i) individual anions, (ii) individual cations, (iii) ion pairs, (iv) acetic acid as a reference carboxyl species, and (v) the halohydrin intermediate formed in the oxirane ring-opening reaction by the anion.[31] Moreover, the structure, length of the shortest bond and binding energies of the neat ILs at the relaxed state are displayed in Figure 1.

The HOMO was calculated to define the energy of the most loosely bound electron (at the highest occupied molecular orbital), and the likelihood of a cation formation. Low HOMO species, such as CH_2CO_2HMIm and CH_2CO_2MIm, indicate a high likelihood to provide electrons to neighboring chemical species. In the same way, we calculated the LUMO to determine the chemical species that will most likely receive electrons. When a low-LUMO and a low-HOMO species are close, a bond is formed quantified by the high E_b and low binding distance (d). In fact, the reactivity of these chemical species can be quantitatively determined through η, where low-η (soft) species are more reactive than high-η (hard) species.

The simplest IL structure ($CH_2CO_2HMImCl$) was investigated in more detail to detect the most probable species promoting the reaction with PGE. Thus, the E_b, HOMO, LUMO, and η were evaluated for four possible conditions that the IL could present during the reaction: (i) its native cation and anion, (ii) its native cation apart from its anion, (iii) a deprotonated cation with the native anion, and (iv) its zwitterionic species, as shown in Figure 10. Moreover, the values for the halohydrin intermediate were also presented (Figure 10). It can be clearly evidenced in Table 2 and Figure 10b that $CH_2CO_2HMImCl$ is able of forming both a very reactive (soft species), represented by the loss of its anion (Figure 10b, Table 2 No. 4), and a less reactive (hard) species, represented by the loss of both its anion and the carboxylic proton (Figure 10d, Table 2 No. 5). This would mean that, if the proton reacts in the first reaction step, then a hard species (consisting on a six atom h-bonded cyclic structure stabilizing a zwitterion) would be formed (Figure 10d), most likely seizing the reaction.

Interestingly, the two hardest species derived from $CH_2CO_2HMImCl$, as predicted by DFT, are carboxylate anion cyclic structures based on strong intramolecular ionic and doubly ionic H-bonding (Figure 10c and d), which is a known cause of η increasing in ILs.[38] Both of this species are exclusively possible to form in the ILs with short aliphatic cation side-chain, namely, $CH_2CO_2HMImCl$, $CH_2CO_2HMImNTf_2$, and $(CH_2CO_2H)_2ImCl$, due to the fixed proximity between the carboxyl group with the imidazolium ring.

The formation of these hard planar structures could be the reason for both the detection of carboxylate anion stabilization and the stacked-cluster IL structures, evidenced by MALDI-TOF analysis of the neat ILs (Figures S5 and S6). However, after reacting with PGE, both carboxylate anions (Figures S12 and S13) and stacked structures (Figures S14 and S16) were mainly detected for Cl^- anion-based ILs, even at 100 °C, suggesting a strong anion-dependent stabilization of these species.

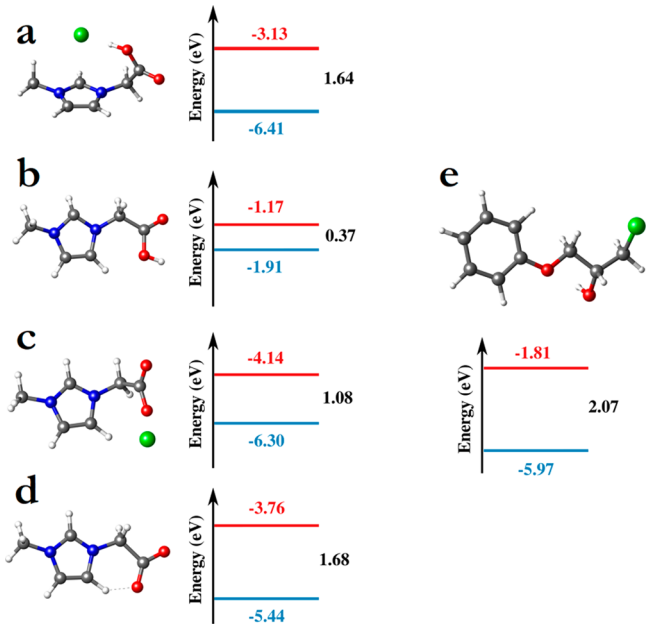

Figure 10. Optimized structures from DFT calculations and energy diagram for four possible conditions of $CH_2CO_2HMImCl$; $CH_2CO_2HMImCl$ (a), CH_2CO_2HMIm (b), CH_2CO_2MImCl (c), CH_2CO_2MIm (d), and the PGE-IL halohydrin reaction intermediate (e). HOMO energies are shown in blue, LUMO energies in red, and chemical hardness in black.

It is worth mentioning that no direct correlation between the native ILs' η and the reactions rate/yield was found, besides the similar rate/yield increase with increasing the reaction temperature or individual increase of one of these components with η decrease (Figure S18). That was somehow expected since a direct correlation would be obtained only for reactions with one variable, consisting in only one step, with monofunctional ILs, since once the first functional group would react a new η would be obtained. Simulations of the individual intermediates, as performed for $CH_2CO_2HMImCl$ will be necessary for obtaining reliable correlations at each reaction step. For this reason, we used the η values only as a comparative approach to direct to the most favorable reaction pathway for a specific IL, which was interpreted stepwise.

Reaction Mechanism: Proposed Pathway Based on the Experimental and the Theoretical Data. As previously described, there are apparently two different mechanisms ruling the reaction outcomes that are dependent on the IL's anion. These mechanisms seem to be specifically dependent on the anions' steric hindrance and nucleophilicity, and they were further defined as *nucleophilic* and *basic catalysis* (Figure 11).

First, in accordance with previously published results,[30,31] Cl^- anion-based ILs seem to follow a nucleophilic catalysis pathway, i.e., the oxirane ring is activated by the acidic proton from the IL's carboxyl group, while the IL's Cl^- anion acts as a nucleophilic agent in the ring opening reaction, forming a halohydrin (Figure 11, nucleophilic catalysis). At this point, two possible reaction paths could be followed, involving a nucleophilic attack on the halohydrin's carbon associated with the Cl, releasing the Cl once again as an anion, which could be

DOI: 10.1021/acssuschemeng.9b04810
ACS Sustainable Chem. Eng. 2019, 7, 19050−19061

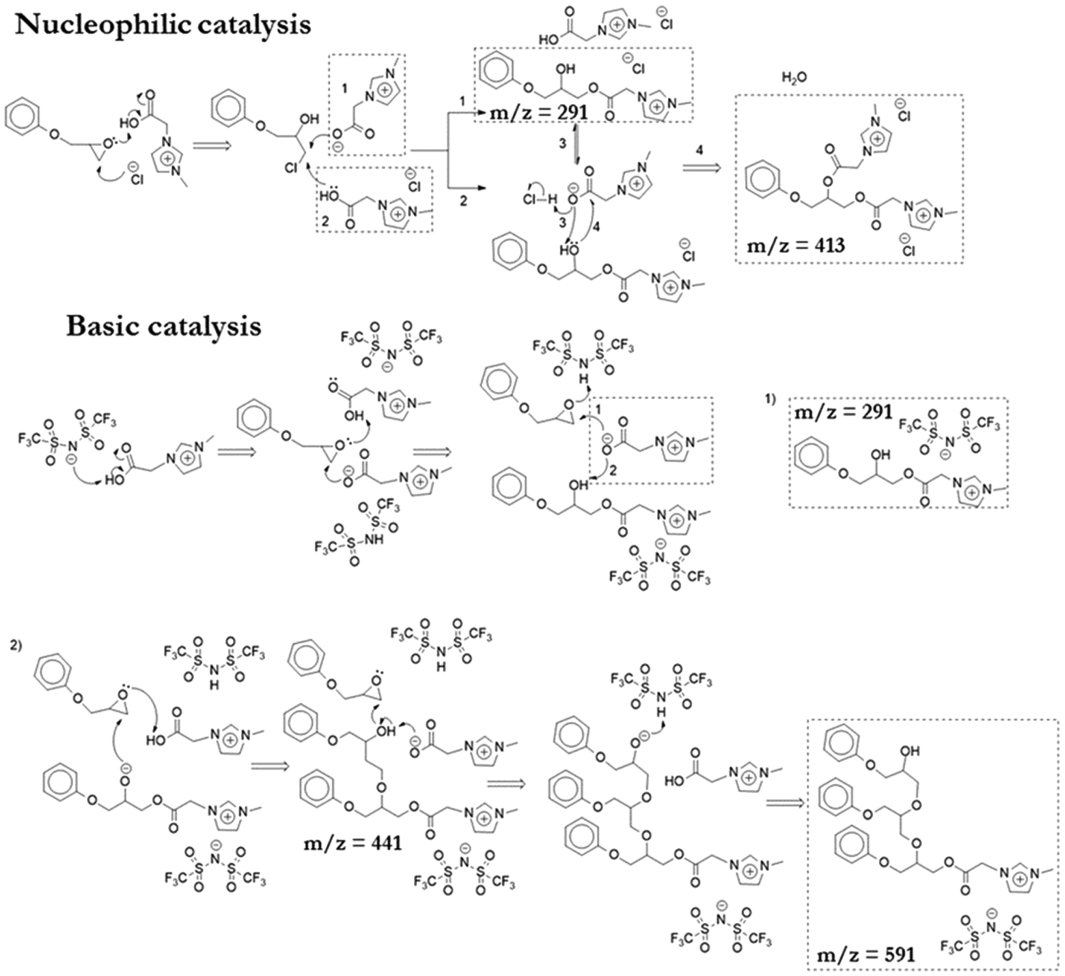

Figure 11. Proposed nucleophilic and basic catalysis mechanisms for the PGE-IL coupling processes via PGE epoxide ring-opening.

performed by (i) the zwitterionic species formed by the IL's proton loss (Figure 11, reaction path 1); or (ii) an unreacted carboxy-IL (Figure 11, reaction path 2).

Considering the η, as calculated by DFT, path 2 is favored since the IL's protonated structure (Figure 10b) is more reactive than the zwitterionic one (which stabilizes itself by intramolecular H-bonding, Figure 10d). Therefore, once again two outcomes are possible: (i) the zwitterionic species react with the HCl formed in the step before and the reaction is finished with a PGE-IL single coupling (Figure 11, path 3), corroborating with MALDI-TOF and NMR results (m/z = 291, Figures 3c and 4a); or (ii) the zwitterionic species react with the PGE-IL coupled species, forming a second coupling (via condensation esterification) reaction between another IL and PGE-IL (Figure 11, path 4), which seems to be promoted by the higher temperature since it was obtained only in small amounts when $CH_2CO_2HMImCl$ was reacted with PGE at 100 °C (m/z = 413, Figure 3d).

Interestingly, a different reaction mechanism was observed when the NTf_2^- anion was present in the reaction with PGE. In this case, the IL's anion seems to act as a Brønsted base, rather than a nucleophile, deprotonating the IL's carboxyl group and converting it into a reactive carboxylate anion, which could react with PGE assisted by another IL's cation (Figure 11, basic catalysis). This mechanism shift based on the base character of the IL anion was already reported by Binks et al.,[39] however, they reported on nonfunctionalized ILs where the basic anion subtracts the proton from the imidazolium ring's C2-carbon, activating a carbene-based mechanism. However, for the Brønsted-acidic ILs, the available carboxyl proton seems to be prioritized. For this to be possible, one must consider that NTf_2^- forms $HNTf_2$ as the conjugated acid, which is a strong acid in water (making NTf_2^- a week base). But its behavior is much more complex in partially- or nonaqueous media since it does not deprotonate water when in the presence of some organic compounds,[40] and it is acidity is weaker when dissolved in carboxylic acids, e.g., pK_a = 7.8 in acetic acid,[41] which could allow the NTf_2^- behavior as a considerably active base.

At this point, two outcomes are possible: (i) activation of a new oxirane ring by the proton previously captured by the NTf_2^- anion and ring-opening by the nucleophilic attack of the zwitterionic species on the oxirane ring's carbon (Figure 11, basic mechanism, reaction path 1), forming single PGE-IL couplings (m/z = 291, Figure 3c); (ii) the zwitterionic species attack the hydroxyl moieties formed by the epoxide ring-opening, producing an alkoxide species that could react with the next PGE molecule (Figure 11, basic catalysis, reaction path 2). Through this reaction path, after the formation of a PGE dimer (m/z = 441, Figure 3g), the reaction could be finished if the oxirane ring would attack the proton previously captured by the NTf_2^- anion. However, it could also continue aggregating PGE molecules if the oxirane ring would be once again activated by the carboxy-IL, allowing the attack on a new

DOI: 10.1021/acssuschemeng.9b04810
ACS Sustainable Chem. Eng. 2019, 7, 19050−19061

PGE molecule and forming trimeric species (m/z = 591, Figure 3h), matching perfectly with the MALDI-TOF results.

It is worth noting that most of the dimeric and trimeric species were obtained in small amounts (Table 1), however, they were pivotal to indicate the different mechanism pathways for obtaining the different coupling reaction products. Using the information presented in this study for process optimizations could allow obtaining suitable products in larger amounts for practical use.

CONCLUSIONS

The mono-, bi-, and tetra-functionalized (with carboxyl groups) ILs used in this study presented anion dependent reactivity with PGE, and the fastest epoxide ring-opening process and the most effective for coupling with PGE was observed for a system with a monofunctional IL containing the Cl^- anion ($C_3H_6CO_2HMImCl$).

At 25 °C both monofunctional-IL systems based on Cl anion ($CH_2CO_2HMImCl$ and $C_3H_6CO_2HMImCl$) promoted at least 98% epoxy consumption but less than 46% conversion into the PGE-IL coupling products after 48 h, with the majority of these ILs' cations remaining in their monomeric, stacked clusters (partially stabilizing their zwitterionic forms) or zwitterionic species stabilized by the coupling product. The IL stacking into clusters via hydrogen bonding, C−H−π interactions and $\pi-\pi$ stacking was demonstrated by NMR and MALDI-TOF, which presented multiples of the mass of a deprotonated IL cation, evidencing the formation of zwitterionic IL species, which were also observed by FTIR. The cluster sizes vary with the IL structure, always presenting a total charge +1 due to the presence of one unaltered cationic species. The temperature increase to 100 °C for these reactions partially disrupted the IL stacking and increased the yield to ∼100% epoxy consumption and ∼92% conversion into the PGE-IL coupling products in only 10−20 min of the reaction, also forming a product of a second IL cation insertion, probably via condensation esterification reaction. The reaction between PGE and $CH_2CO_2HMImNTf_2$, containing the bulky NTf_2^- anion presented a different behavior to that of ILs with Cl^- anion, without zwitterionic species and cluster formation. Moreover, the same IL reacted with PGE forming small amounts of dimers and trimers of PGE via etherification reaction, suggesting two different anion dependent mechanisms, herein referred as Nucleophilic and Basic catalysis.

The use of dicarboxylic ILs, although with a break of the stoichiometry between epoxy and carboxylic groups, also presented good performances and the $(Benzoic)_2ImCl$ was more effective than $(CH_2CO_2H)_2ImCl$ with about 71% conversion to coupling products and ∼78% of those were products with both carboxylic groups reacted (disubstituted) in less than 12 h. Surprisingly, the tetracarboxylic $(Isophtalic)_2ImCl$) presented, after 12 h of reaction, an even higher conversion than $(Benzoic)_2ImCl$ but with a mixture of mono-, di-, tri-, and tetra- substituted products, where almost 50% of the product is tetra-substituted.

The model reactions between PGE and acetic acid demonstrated the stoichiometry and intramolecular catalysis contributions, where the addition of only acetic acid to PGE caused no reaction but the addition of a "non-functionalized IL" started the reaction, with considerable increased of its rate at an equimolar acetic acid/IL ratio. Nevertheless, although creating the same condition as the most effective reaction detected for carboxylic ILs, when the intermolecular catalysis is forced the reaction rate is smaller. Moreover, the use of DFT demonstrated to be a good tool to help unveiling the reaction mechanism by observing the reactivity of the possible intermediates. Interestingly, the two hardest species derived from $CH_2CO_2HMImCl$, as predicted by DFT, are carboxylate anion cyclic structures based on strong intramolecular ionic and doubly ionic H-bonding, demonstrating a strong anion-dependent stabilization of these species.

Altogether, this study provided tools for the preparation of a countless number of formulations between epoxides and carboxylates using an IL platform. This platform is expected to be useful for reactions from small molecules coupling to polymerization and cross-linking processes that fulfill most of the 12 principles of green chemistry, including; prevention of waste and atom economy (water is the only residue), low toxicity reactants and products, solvent-free, energy efficient (mostly RTP conditions), one-pot reaction, and metal-catalyst free. Moreover, the theoretical−experimental correlations allow predicting not only the reactivity of the systems but also the most appropriate intermediates to be achieved, and the all-in-one catalyst characteristic of these ILs allow an IL-structure dependent outcome of the products, which may be used in complex system with considerable selectivity.

ASSOCIATED CONTENT

Supporting Information

The Supporting Information is available free of charge on the ACS Publications website at DOI: 10.1021/acssuschemeng.9b04810.

Further details of the imidazolium salts' synthesis protocols and extensive NMR, FTIR, and MALDI-TOF characterization of reactants and products (PDF)

AUTHOR INFORMATION

Corresponding Authors

*E-mail: benesh@imc.cas.cz (H.B.).
*E-mail: donato@imc.cas.cz (R.K.D.).

ORCID

Magdalena Perchacz: 0000-0002-1803-7771
Leandro Seixas: 0000-0001-7420-0708
Sebastien Livi: 0000-0003-4959-982X
Hynek Beneš: 0000-0002-6861-1997
Ricardo K. Donato: 0000-0002-7216-7120

Notes

The authors declare no competing financial interest.

ACKNOWLEDGMENTS

This research was funded by the Czech Science Foundation, grant no. 17-08273S, and the Ministry of Education, Youth and Sports of CR, project POLYMAT LO1507. The authors are thankful to Zuzana Walterová for the MALDI-TOF MS measurements. L.S. acknowledges the financial support from CNPq (Brazil), and the use of the computational facilities from NACAD/COPPE/UFRJ.

REFERENCES

(1) Matějka, L.; Pokorný, S.; Dušek, K. Network formation involving epoxide and carboxyl groups. *Polym. Bull.* **1982**, *7*, 123−128.
(2) Montarnal, D.; Capelot, M.; Tournilhac, F.; Leibler, L. Silica-Like Malleable Materials from Permanent Organic Networks. *Science* **2011**, *334*, 965−968.

DOI: 10.1021/acssuschemeng.9b04810
ACS Sustainable Chem. Eng. 2019, 7, 19050−19061

(3) Dupont, J.; de Souza, R. F.; Suarez, P. A. Z. Ionic Liquid (Molten Salt) Phase Organometallic Catalysis. *Chem. Rev.* **2002**, *102*, 3667−3692.
(4) Welton, T. Room-Temperature Ionic Liquids. Solvents for Synthesis and Catalysis. *Chem. Rev.* **1999**, *99*, 2071−2083.
(5) Maka, H.; Spychaj, T.; Pilawka, R. Epoxy Resin/Ionic Liquid Systems: The Influence of Imidazolium Cation Size and Anion Type on Reactivity and Thermomechanical Properties. *Ind. Eng. Chem. Res.* **2012**, *51*, 5197−5206.
(6) Maka, H.; Spychaj, T.; Zenker, M. High performance epoxy composites cured with ionic liquids. *J. Ind. Eng. Chem.* **2015**, *31*, 192−198.
(7) Perchacz, M.; Donato, R. K.; Seixas, L.; Zhigunov, A.; Konefał, R.; Serkis-Rodzeń, M.; Beneš, H. Ionic Liquid-Silica Precursors via Solvent-Free Sol−Gel Process and Their Application in Epoxy-Amine Network: A Theoretical/Experimental Study. *ACS Appl. Mater. Interfaces* **2017**, *9*, 16474−16487.
(8) Donato, K. Z.; Matějka, L.; Mauler, R. S.; Donato, R. K. Recent Applications of Ionic Liquids in the Sol-Gel Process for Polymer−Silica Nanocomposites with Ionic Interfaces. *Colloids Interfaces* **2017**, *1*, 5.
(9) Kalista, S. J.; Pflug, J. R.; Varley, R. J. Effect of ionic content on ballistic self-healing in EMAA copolymers and ionomers. *Polym. Chem.* **2013**, *4*, 4910−4926.
(10) Ponyrko, S.; Donato, R. K.; Matějka, L. Tailored high performance shape memory epoxy−silica nanocomposites. Structure design. *Polym. Chem.* **2016**, *7*, 560−572.
(11) Das, A.; Sallat, A.; Böhme, F.; Suckow, M.; Basu, D.; Wießner, S.; Stöckelhuber, W.; Voit, B.; Heinrich, G. Ionic Modification Turns Commercial Rubber into a Self-Healing Material. *ACS Appl. Mater. Interfaces* **2015**, *7*, 20623−20630.
(12) Donato, K. Z.; Lavorgna, M.; Donato, R. K.; Raucci, M. G.; Buonocore, G. G.; Ambrosio, L.; Schrekker, H. S.; Mauler, R. S. High Amorphous Vinyl Alcohol-Silica Bionanocomposites: Tuning Interface Interactions with Ionic Liquids. *ACS Sustainable Chem. Eng.* **2017**, *5*, 1094−1105.
(13) Donato, R. K.; Matejka, L.; Schrekker, H. S.; Plestil, J.; Jigounov, A.; Brus, J.; Slouf, M. The multifunctional role of ionic liquids in the formation of epoxy-silica nanocomposites. *J. Mater. Chem.* **2011**, *21*, 13801−13810.
(14) Donato, R. K.; Donato, K. Z.; Schrekker, H. S.; Matějka, L. Tunable reinforcement of epoxy-silica nanocomposites with ionic liquids. *J. Mater. Chem.* **2012**, *22*, 9939−9948.
(15) Nguyen, T. K. L.; Livi, S.; Soares, B. G.; Benes, H.; Gérard, J.-F.; Duchet-Rumeau, J. Toughening of Epoxy/Ionic Liquid Networks with Thermoplastics Based on Poly(2,6-dimethyl-1,4-phenylene ether) (PPE). *ACS Sustainable Chem. Eng.* **2017**, *5*, 1153−1164.
(16) Nguyen, T. K. L.; Soares, B. G.; Duchet-Rumeau, J.; Livi, S. Dual functions of ILs in the core-shell particle reinforced epoxy networks: Curing agent vs dispersion aids. *Compos. Sci. Technol.* **2017**, *140*, 30−38.
(17) Livi, S.; Chardin, C.; Lins, L. C.; Halawani, N.; Pruvost, S.; Duchet-Rumeau, J.; Gerard, J.-F.; Baudoux, J. From Ionic Liquid Epoxy Monomer to Tunable Epoxy−Amine Network: Reaction Mechanism and Final Properties. *ACS Sustainable Chem. Eng.* **2019**, *7*, 3602−3613.
(18) Odent, J.; Raquez, J.-M.; Samuel, C.; Barrau, S.; Enotiadis, A.; Dubois, P.; Giannelis, E. P. Shape-Memory Behavior of Polylactide/Silica Ionic Hybrids. *Macromolecules* **2017**, *50*, 2896−2905.
(19) Odent, J.; Raquez, J.-M.; Dubois, P.; Giannelis, E. P. Ultra-stretchable ionic nanocomposites: from dynamic bonding to multi-responsive behavior. *J. Mater. Chem. A* **2017**, *5*, 13357−13363.
(20) Donato, R. K.; Perchacz, M.; Ponyrko, S.; Donato, K. Z.; Schrekker, H. S.; Beneš, H.; Matějka, L. Epoxy−silica nanocomposite interphase control using task-specific ionic liquids via hydrolytic and non-hydrolytic sol−gel processes. *RSC Adv.* **2015**, *5*, 91330−91339.
(21) Serier, A.; Pascault, J. P.; My, L. T. Reactions in aminosilane−epoxy prepolymer systems I. Kinetics of epoxy−amine reactions. *J. Polym. Sci., Part A: Polym. Chem.* **1991**, *29*, 209−218.
(22) Fei, Z.; Zhao, D.; Geldbach, T. J.; Scopelliti, R.; Dyson, P. J. Brønsted Acidic Ionic Liquids and Their Zwitterions: Synthesis, Characterization and pKa Determination. *Chem. - Eur. J.* **2004**, *10*, 4886−4893.
(23) Sen, S.; Nair, N. N.; Yamada, T.; Kitagawa, H.; Bharadwaj, P. K. High Proton Conductivity by a Metal−Organic Framework Incorporating Zn_8O Clusters with Aligned Imidazolium Groups Decorating the Channels. *J. Am. Chem. Soc.* **2012**, *134*, 19432−19437.
(24) Sen, S.; Neogi, S.; Aijaz, A.; Xu, Q.; Bharadwaj, P. K. Construction of Non-Interpenetrated Charged Metal−Organic Frameworks with Doubly Pillared Layers: Pore Modification and Selective Gas Adsorption. *Inorg. Chem.* **2014**, *53*, 7591−7598.
(25) Soler, J. M.; Artacho, E.; Gale, J. D.; García, A.; Junquera, J.; Ordejón, P.; Sánchez-Portal, D. The SIESTA method for ab initio order-N materials simulation. *J. Phys.: Condens. Matter* **2002**, *14*, 2745−2779.
(26) Troullier, N.; Martins, J. L. Efficient pseudopotentials for plane-wave calculations. *Phys. Rev. B: Condens. Matter Mater. Phys.* **1991**, *43*, 1993−2006.
(27) Vydrov, O. A.; van Voorhis, T. Nonlocal van der Waals density functional: The simpler the better. *J. Chem. Phys.* **2010**, *133*, 244103.
(28) Boys, S. F.; Bernardi, F. The calculation of small molecular interactions by the differences of separate total energies. Some procedures with reduced errors. *Mol. Phys.* **1970**, *19*, 553−566.
(29) González, M. G.; Cabanelas, J. C.; Baselga, J. Applications of FTIR on Epoxy Resins-Identification, Monitoring the Curing Process, Phase Separation and Water Uptake. In *Infrared Spectroscopy: Materials Science, Engineering and Technology*, Vol. *14*; Theophile, T., Ed.; Intech Open, 2012; pp 261−284 (DOI: 10.5772/2055).
(30) Binks, F. C.; Cavalli, G.; Henningsen, M.; Howlin, B. J.; Hamerton, I. Examining the Influence of Anion Nucleophilicity on the Polymerisation Initiation Mechanism of Phenyl Glycidyl Ether. *Polymers* **2019**, *11*, 657.
(31) Ranu, B. C.; Banerjee, S. Ionic Liquid as Reagent. A Green Procedure for the Regioselective Conversion of Epoxides to Vicinal-Halohydrins Using [AcMIm]X under Catalyst-and Solvent-Free Conditions. *J. Org. Chem.* **2005**, *70*, 4517−4519.
(32) Kolev, T.; Spiteller, M.; Koleva, B. Spectroscopic and structural elucidation of amino acid derivatives and small peptides: experimental and theoretical tools. *Amino Acids* **2010**, *38*, 45−50.
(33) Dupont, J.; Suarez, P. A. Z.; de Souza, R. F.; Burrow, R. A.; Kintzinger, J.-P. C-H-π Interactions in 1-Butyl-3-methylimidazolium Tetraphenylborate Molten Salt: Solid and Solution Structures. *Chem. - Eur. J.* **2000**, *6*, 2377−2381.
(34) Dupont, J. On the solid, liquid and solution structural organization of imidazolium ionic liquids. *J. Braz. Chem. Soc.* **2004**, *15*, 341−350.
(35) Mele, A.; Romanò, G.; Giannone, M.; Ragg, E.; Fronza, G.; Raos, G.; Marcon, V. The local structure of ionic liquids: cation-cation NOE interactions and internuclear distances in neat [BMIM][BF_4] and [BDMIM][BF_4]. *Angew. Chem., Int. Ed.* **2006**, *45*, 1123−1126.
(36) Max, J.-J.; Chapados, C. Infrared Spectroscopy of Aqueous Carboxylic Acids: Comparison between Different Acids and Their Salts. *J. Phys. Chem. A* **2004**, *108*, 3324−3337.
(37) Ohtani, H.; Ishimura, S.; Kumai, M. Thermal decomposition behaviors of imidazolium-type ionic liquids studied by pyrolysis-gas chromatography. *Anal. Sci.* **2008**, *24*, 1335−1340.
(38) Hunt, P. A.; Ashworth, C. R.; Matthews, R. P. Hydrogen bonding in ionic liquids. *Chem. Soc. Rev.* **2015**, *44*, 1257−1288.
(39) Binks, F. C.; Cavalli, G.; Henningsen, M.; Howlin, B. J.; Hamerton, I. Investigating the mechanism through which ionic liquids initiate the polymerisation of epoxy resins. *Polymer* **2018**, *139*, 163−176.
(40) Stoyanov, E. S.; Kim, K.-C.; Reed, C. A. A Strong Acid that Does Not Protonate Water. *J. Phys. Chem. A* **2004**, *108*, 9310−9315.
(41) Foropoulos, J., Jr.; DesMarteau, D. D. Synthesis, properties, and reactions of bis((trifluoromethyl)sulfonyl) imide, $(CF_3SO_2)_2NH$. *Inorg. Chem.* **1984**, *23*, 3720−3723.

DOI: 10.1021/acssuschemeng.9b04810
ACS Sustainable Chem. Eng. 2019, 7, 19050−19061